PROCEEDINGS OF SCIENCE

Ω_{bbb} excited-state spectroscopy from lattice QCD

Stefan Meinel*
Center for Theoretical Physics,
Massachusetts Institute of Technology,
Cambridge, MA 02139, USA
E-mail: smeinel@mit.edu

Triply heavy baryons are very interesting systems analogous to heavy quarkonia, but are difficult to access experimentally. Lattice QCD can provide precise predictions for these systems, which can be compared to other theoretical approaches. In this work, the spectrum of excited states of the Ω_{bbb} baryon is calculated using lattice NRQCD for the b quarks, and using a domain-wall action for the u, d and s sea quarks. The calculations are done for multiple values of the sea-quark masses, and for two different lattice spacings. The energies of states with angular momentum up to $J = 7/2$ are calculated, and the effects of rotational symmetry breaking by the lattice are analyzed. Precise results are obtained even for the small spin-dependent energy splittings, and the contributions of individual NRQCD interactions to these energy splittings are studied. The results are compared to potential-model calculations.

Xth Quark Confinement and the Hadron Spectrum,
October 8-12, 2012
TUM Campus Garching, Munich, Germany

*Speaker.

PoS(Confinement X)140

1. Introduction

The *bbb* system can be viewed as the baryonic analogue of the bottomonium system. Like bottomonia, *bbb* baryons are governed by multiple well-separated energy scales and are therefore amenable to the description with effective field theories [1]. Baryons exhibit the $SU(3)$ gauge symmetry of QCD more directly than mesons, and are sensitive to the resulting genuine three-body forces. Triply heavy baryons probe the three-quark interactions at relatively short distances, where contact with perturbation theory can be made [2].

The aim of the work reported here is to complement the perturbative QCD calculations and other theoretical studies of triply heavy baryons with nonperturbative lattice QCD calculations. In Ref. [3], the mass of the ground-state Ω_{bbb} baryon was calculated using lattice QCD to be $14.371 \pm 0.004_{\text{stat}} \pm 0.011_{\text{syst}} \pm 0.001_{\text{exp}}$ GeV. This was followed by a lattice QCD calculation of Ω_{bbb} excited states in Ref. [4], which is summarized here. Like the bottomonium spectrum, the *bbb* spectrum features a hierarchy of radial/orbital excitations and spin-dependent energy splittings. In Ref. [4], the energies of ten *bbb* excited states where calculated with high precision, resolving even the smallest spin-dependent energy splittings. The calculation includes dynamical u, d, and s sea quarks, and was done at two different lattice spacings of approximately 0.11 fm and 0.08 fm. For lattice spacings of this order, the b quarks can be implemented accurately using lattice NRQCD [5]. With lattice NRQCD it is also possible to study individually the effects of the different spin-dependent interactions in the effective field theory on the *bbb* energy splittings.

2. Lattice actions

The lattice gauge-field configurations used in this work to perform the path integral were generated by the RBC/UKQCD collaboration and are described in Ref. [6]. These configurations include the vacuum-polarization effects of the light and strange quarks. The Iwasaki discretization was chosen for the gauge action, and the u, d, and s quarks were implemented using a domain-wall action that preserves chiral symmetry even at nonzero lattice spacing. The main parameters of the ensembles are given in Table 1.

$L^3 \times T$	β	$am_{u,d}$	am_s	am_b	a [fm]	m_π [GeV]
$24^3 \times 64$	2.13	0.005	0.04	2.487	0.1119(17)	0.3377(54)
$24^3 \times 64$	2.13	0.01	0.04	2.522	0.1139(19)	0.4194(70)
$24^3 \times 64$	2.13	0.02	0.04	2.622	0.1177(29)	0.541(14)
$24^3 \times 64$	2.13	0.03	0.04	2.691	0.1196(29)	0.641(15)
$32^3 \times 64$	2.25	0.004	0.03	1.831	0.0849(12)	0.2950(40)
$32^3 \times 64$	2.25	0.006	0.03	1.829	0.0848(17)	0.3529(69)
$32^3 \times 64$	2.25	0.008	0.03	1.864	0.0864(12)	0.3950(55)

Table 1: The lattice sizes, the gauge couplings ($\beta = 6/g^2$), the quark masses, and the corresponding lattice spacings and pion masses.

In the following, we denote the b-quark field by ψ. Similarly to Ref. [5], the lattice NRQCD action is written as

$$S_\psi = a^3 \sum_{\mathbf{x},t} \psi^\dagger(\mathbf{x},t) \left[\psi(\mathbf{x},t) - \left(1 - \frac{a\,\delta H}{2}\right) \left(1 - \frac{aH_0}{2n}\right)^n U_4^\dagger \left(1 - \frac{aH_0}{2n}\right)^n \left(1 - \frac{a\,\delta H}{2}\right) \psi(\mathbf{x},t-a) \right], \tag{2.1}$$

where U_4 are the temporal gauge links, and H_0 and δH are given by

$$\begin{aligned}
H_0 &= -\frac{\Delta^{(2)}}{2m_b}, \\
\delta H &= -c_1 \frac{\left(\Delta^{(2)}\right)^2}{8m_b^3} + c_2 \frac{ig}{8m_b^2} \left(\widetilde{\boldsymbol{\nabla}} \cdot \widetilde{\mathbf{E}} - \widetilde{\mathbf{E}} \cdot \widetilde{\boldsymbol{\nabla}}\right) - c_3 \frac{g}{8m_b^2} \boldsymbol{\sigma} \cdot \left(\widetilde{\boldsymbol{\nabla}} \times \widetilde{\mathbf{E}} - \widetilde{\mathbf{E}} \times \widetilde{\boldsymbol{\nabla}}\right) - c_4 \frac{g}{2m_b} \boldsymbol{\sigma} \cdot \widetilde{\mathbf{B}} \\
&\quad + c_5 \frac{a^2 \Delta^{(4)}}{24 m_b} - c_6 \frac{a \left(\Delta^{(2)}\right)^2}{16 n m_b^2} \\
&\quad - c_7 \frac{g}{8m_b^3} \left\{ \Delta^{(2)}, \boldsymbol{\sigma} \cdot \widetilde{\mathbf{B}} \right\} - c_8 \frac{3g}{64 m_b^4} \left\{ \Delta^{(2)}, \boldsymbol{\sigma} \cdot \left(\widetilde{\boldsymbol{\nabla}} \times \widetilde{\mathbf{E}} - \widetilde{\mathbf{E}} \times \widetilde{\boldsymbol{\nabla}}\right) \right\} - c_9 \frac{ig^2}{8m_b^3} \boldsymbol{\sigma} \cdot (\widetilde{\mathbf{E}} \times \widetilde{\mathbf{E}}).
\end{aligned} \tag{2.2}$$

The different terms in the NRQCD action are suppressed by different powers of v, the average speed of the b quarks inside the hadron. The leading term, H_0, is of order v^2, and gives the dominant contribution to radial/orbital energy splittings in the $b\bar{b}$ and bbb systems. The terms with coefficients $c_{1,2,3,4}$ are the relativistic corrections of order v^4, and the terms with coefficients $c_{7,8,9}$ are relativistic corrections of order v^6 (only the spin-dependent order-v^6 terms are included). The terms with coefficients $c_{5,6}$, which contain powers of the lattice spacing, reduce discretization errors and are not present in the continuum NRQCD action. Because spin splittings first arise at order v^4 through the operators $\boldsymbol{\sigma} \cdot \left(\widetilde{\boldsymbol{\nabla}} \times \widetilde{\mathbf{E}} - \widetilde{\mathbf{E}} \times \widetilde{\boldsymbol{\nabla}}\right)$ and $\boldsymbol{\sigma} \cdot \widetilde{\mathbf{B}}$, the matching coefficients c_3 and c_4 of these operators were tuned nonperturbatively to achieve high precision [4]. The other matching coefficients were set to their tree-level values, $c_i = 1$.

3. Construction of bbb operators

The bbb energies can be extracted from Euclidean two-point functions of interpolating operators Ω_r^Λ with the desired quantum numbers of the bbb states on the lattice. These operators were constructed starting from Gaussian-smeared b quark fields

$$\tilde{\psi}_{a\alpha} = \left[\left(1 + \frac{r_S^2}{2n_S} \Delta^{(2)}\right)^{n_S} \psi \right]_{a\alpha}, \tag{3.1}$$

where $a = 1,2,3$ is the color index, $\alpha = \uparrow, \downarrow$ is the spin index, $\Delta^{(2)}$ is a gauge-covariant lattice Laplace operator, and the smearing radius was chosen to be $r_S \approx 0.14$ fm. To obtain a nontrivial spatial structure, up to 2 gauge-covariant derivatives were then applied to obtain the following 13 quark building blocks,

$$\begin{aligned}
\tilde{\psi}_{a\alpha 1} &= \tilde{\psi}_{a\alpha}, \\
\tilde{\psi}_{a\alpha 2} &= (\nabla_x \tilde{\psi})_{a\alpha}, \quad \tilde{\psi}_{a\alpha 3} = (\nabla_y \tilde{\psi})_{a\alpha}, \quad \tilde{\psi}_{a\alpha 4} = (\nabla_z \tilde{\psi})_{a\alpha}, \\
\tilde{\psi}_{a\alpha 5} &= (\nabla_x \nabla_x \tilde{\psi})_{a\alpha}, \quad \tilde{\psi}_{a\alpha 6} = (\nabla_y \nabla_x \tilde{\psi})_{a\alpha}, \quad \ldots, \quad \tilde{\psi}_{a\alpha 13} = (\nabla_z \nabla_z \tilde{\psi})_{a\alpha}.
\end{aligned} \tag{3.2}$$

Using Clebsch-Gordan coefficients, these building blocks were then combined to baryon operators Ω^J_m that would have a definite total angular momentum J in continuous space:

$$\Omega^J_m = \sum_{m_L,m_S} \langle J,m|L,m_L;S,m_S\rangle \; \Gamma_{ijk\,\alpha\beta\gamma}(L,m_L,S,m_S) \; \varepsilon_{abc} \; \tilde{\psi}_{a\alpha i} \, \tilde{\psi}_{b\beta j} \, \tilde{\psi}_{c\gamma k} \, . \tag{3.3}$$

There are multiple ways of combining the spin indices α,β,γ and the derivative indices i,j,k to a given total spin S and total orbital angular momentum L, leading to different types of operators classified by permutation symmetries [7]. With two derivatives, the largest possible value of J is $\frac{7}{2}$.

Next, in order to account for the breaking of rotational symmetry by the lattice, linear combinations of the different m-components of the operators Ω^J_m were formed, such that the resulting operators transform in irreducible representations, Λ, of the double cover of the octahedral group ^{2}O:

$$\Omega^\Lambda_r = \sum_m \mathscr{S}^{J,m}_{\Lambda,r} \, \Omega^J_m . \tag{3.4}$$

The subduction coefficients $\mathscr{S}^{J,m}_{\Lambda,r}$ can be found in Ref. [7]. The index $r = 1...\dim(\Lambda)$ denotes the row of the irrep. The full procedure described in this section produces seven different *bbb* operators in the H_g irrep, three different operators each in the G_{1g} and G_{2g} irreps, and one operator each in the H_u and G_{1u} irreps [4], where the subscripts g/u denote even/odd parity.

4. Data analysis

Using the operators from Eq. (3.4), the row-averaged two-point functions

$$C^{(\Lambda)}_{ij}(t) = \frac{1}{\dim(\Lambda)} \sum_{r=1}^{\dim(\Lambda)} \Big\langle \sum_{\mathbf{x}} \Omega^{\Lambda(i)}_r(\mathbf{x},t) \, \Omega^{\Lambda(j)\dagger}_r(0) \Big\rangle \tag{4.1}$$

were computed. Here, the indices i,j label the different operators constructed in a given irrep Λ. For example, in the G_{1g} irrep, there are three different operators which were constructed using the following values of (L,S,J): $(0,\frac{1}{2},\frac{1}{2})$, $(2,\frac{3}{2},\frac{1}{2})$, and $(2,\frac{3}{2},\frac{7}{2})$. The numerical results for (4.1) were then fitted using the functions

$$C^\Lambda_{ij}(t) = \sum_{n=1}^{N} A^{(\Lambda)}_{n,i} A^{(\Lambda)}_{n,j} \; e^{-E^{(\Lambda)}_n t}, \tag{4.2}$$

where the number of exponentials, N, was chosen equal to the number of operators for each irrep. The full spectral decomposition of $C^\Lambda_{ij}(t)$ also contains an infinite tower of higher excited states, but the starting value of t was chosen large enough such that the contributions from these states are negligible.

Sample fit results for $E^{(\Lambda)}_n$ and $A^{(\Lambda)}_{n,i}$ are shown in Fig. 1. The value of J from which each operator $\Omega^{\Lambda(i)}$ was subduced is also shown. It turns out that for each energy level $E^{(\Lambda)}_n$, the amplitudes $A^{(\Lambda)}_{n,i}$ are large only for one value of J, and this value of J can therefore be assigned to the energy level $E^{(\Lambda)}_n$. The operators retain a strong "memory" of the original value of J [7], and also L and S [4]. Approximately matching energy levels with $J = \frac{5}{2}$ are seen to appear in both the H and G_2 irreps, while approximately matching energy levels with $J = \frac{7}{2}$ appear in all three irreps, as expected.

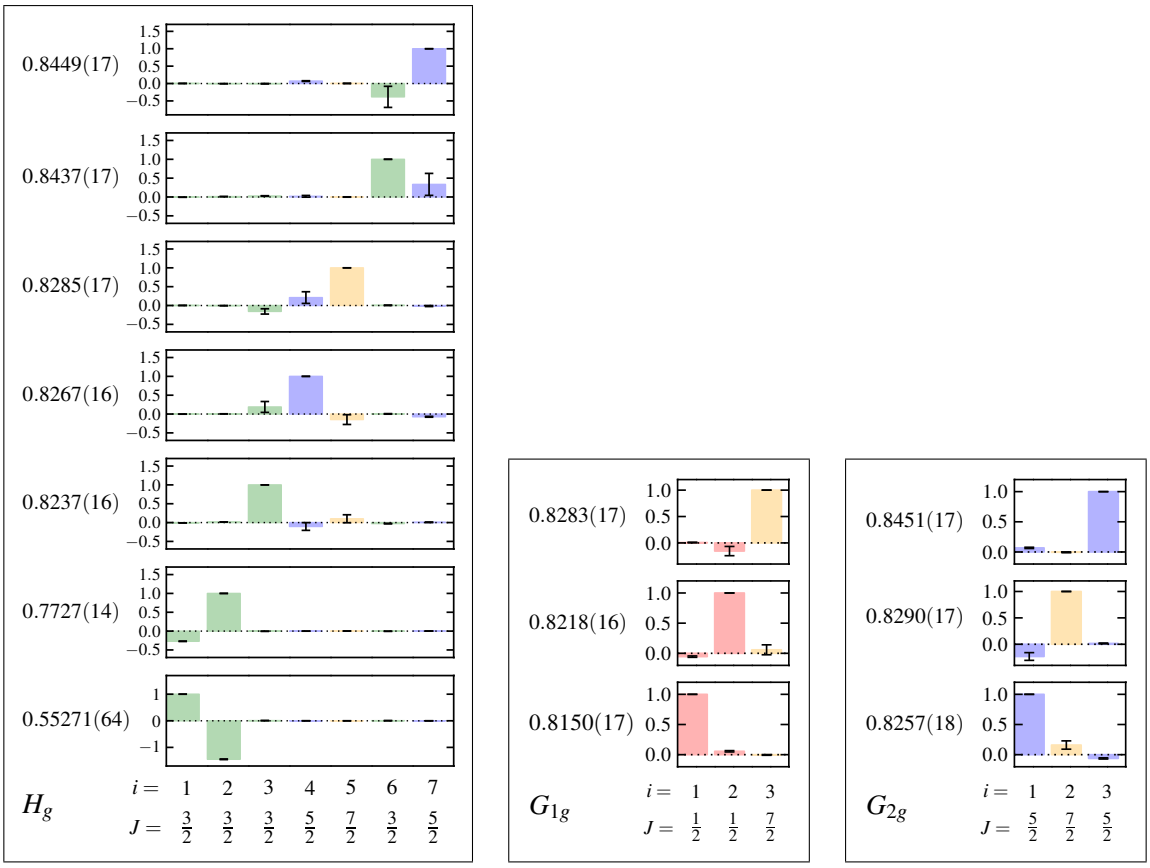

Figure 1: Fitted energies $aE_n^{(\Lambda)}$ and relative amplitudes $A_{n,i}^{(\Lambda)}/A_{n,n}^{(\Lambda)}$ in the H_g, G_{1g}, and G_{2g} irreps. The values of J from which the operators $\Omega^{\Lambda(i)}$ were subduced are indicated below the plots and by the colors. The data shown here are for $a \approx 0.08$ fm, $am_{u,d} = 0.004$.

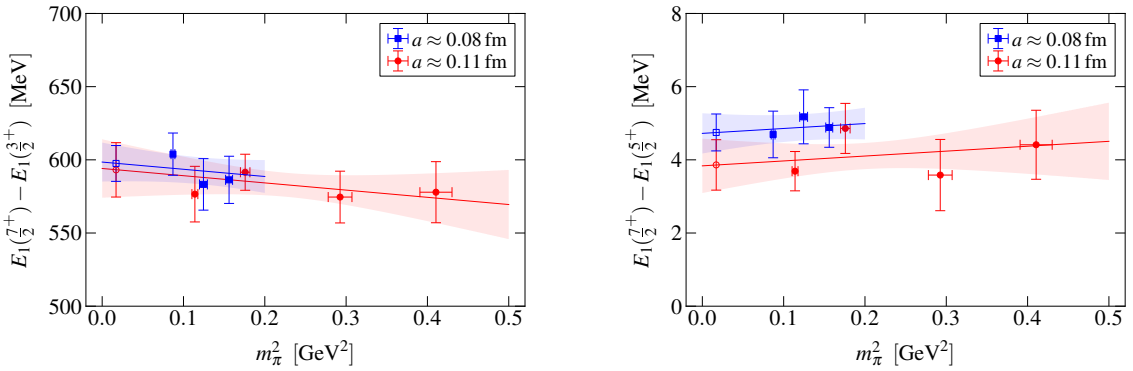

Figure 2: Examples of chiral extrapolations: $E_1(\frac{7}{2}^+) - E_1(\frac{3}{2}^+)$ (left) and $E_1(\frac{7}{2}^+) - E_1(\frac{5}{2}^+)$ (right).

It is shown in Ref. [4] that the small splittings of matching energy levels between the different irreps become smaller when the lattice spacing is reduced, demonstrating the restoration of rotational symmetry. To get the best estimates of the continuum energy levels, simultaneous fits were performed across the different irreps, using common energy parameters for the previously identified matching levels [4]. With the values of J assigned, the energies can then be relabeled as $E_n(J^P)$ by

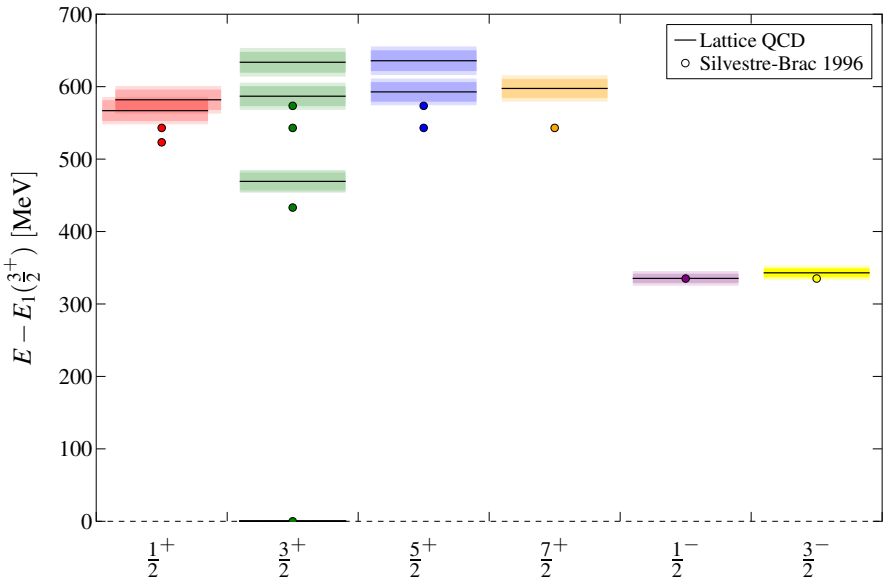

Figure 3: Final results for the *bbb* energy splittings with respect to ground state $E_1(\frac{3}{2}^+)$, compared to the potential-model calculation of Ref. [8]. For the lattice QCD results, the inner shaded bands give the statistical/fitting/scale setting uncertainty, while the outer shaded bands also include the systematic uncertainty. Because the results for the different energy levels are highly correlated, splittings between nearby energy levels can be computed with much smaller absolute uncertainties (see Fig. 4).

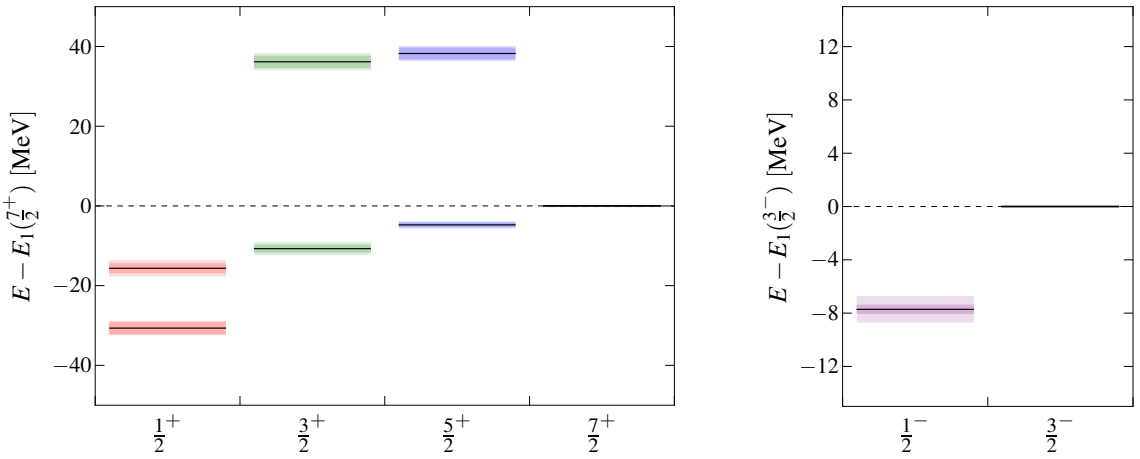

Figure 4: Final results for the *bbb* energy splittings with respect to $E_1(\frac{7}{2}^+)$ (left) and $E_1(\frac{3}{2}^-)$ (right). The inner shaded bands give the statistical/fitting/scale setting uncertainty, while the outer shaded bands also include the systematic uncertainty.

increasing value for each J^P channel. Note that, due to the use of NRQCD, only energy *differences* are physical. The energy differences computed on the various gauge-field ensembles were then extrapolated to the physical value of the pion mass. These extrapolations were done simultaneously for the two different lattice spacings, as shown in Fig. 2. The results at the finer lattice spacing and at the physical pion mass can be taken as the final values for the physical *bbb* spectrum. The remaining systematic uncertainties were estimated individually for each energy splitting in Ref. [4] by considering the contributions of the various NRQCD interaction terms.

In Fig. 3, the final results for the *bbb* energy splittings with respect to the ground state are compared to the potential-model calculation of Ref. [8], where the potential is a sum of two-body interactions and includes spin-spin interactions, but does not include spin-orbit or tensor interactions. For the gross structure of the spectrum, the agreement of this model with the lattice QCD results is remarkably good. However, because the model has no spin-orbit or tensor interactions, it predicts $E_2(\frac{1}{2}^+) = E_3(\frac{3}{2}^+) = E_1(\frac{5}{2}^+) = E_1(\frac{7}{2}^+)$, $E_4(\frac{3}{2}^+) = E_2(\frac{5}{2}^+)$, and $E_1(\frac{1}{2}^-) = E_1(\frac{3}{2}^-)$. As can be seen in Fig. 4, all of these degeneracies are lifted in full QCD.

5. Contributions of individual NRQCD interactions

An interesting question is the following: what are the effects of the different spin-dependent operators in the NRQCD action, Eq. (2.2), on the *bbb* energy splittings? This was investigated in Ref. [4] on one ensemble of gauge configurations ($a \approx 0.11$ fm, $am_{u,d} = 0.005$) by setting different subsets of the NRQCD coefficients, c_i, to zero, and recalculating the *bbb* spectrum in each case. The results are shown here in Fig. 5. In case (a), all spin-dependent interactions are turned off. Up to small corrections caused by the breaking of rotational symmetry on the lattice, this leads to the degeneracies $E_2(\frac{1}{2}^+) = E_3(\frac{3}{2}^+) = E_1(\frac{5}{2}^+) = E_1(\frac{7}{2}^+)$, $E_4(\frac{3}{2}^+) = E_2(\frac{5}{2}^+)$, and $E_1(\frac{1}{2}^-) = E_1(\frac{3}{2}^-)$, which are also present in the potential model of Ref. [8].

In case (b), the operator $\boldsymbol{\sigma} \cdot \widetilde{\mathbf{B}}$ is turned on. Interestingly, the biggest effect is seen for negative-parity energy levels, where this operator introduces a splitting of $E_1(\frac{1}{2}^-) - E_1(\frac{3}{2}^-) = -12.97(45)$ MeV. Note that potential models with both spin-spin and tensor interactions, but without spin-orbit interactions, predict $E_1(\frac{1}{2}^-) - E_1(\frac{3}{2}^-) = 0$ for Ω baryons [9], which suggests that the splitting seen here is of spin-orbit type.

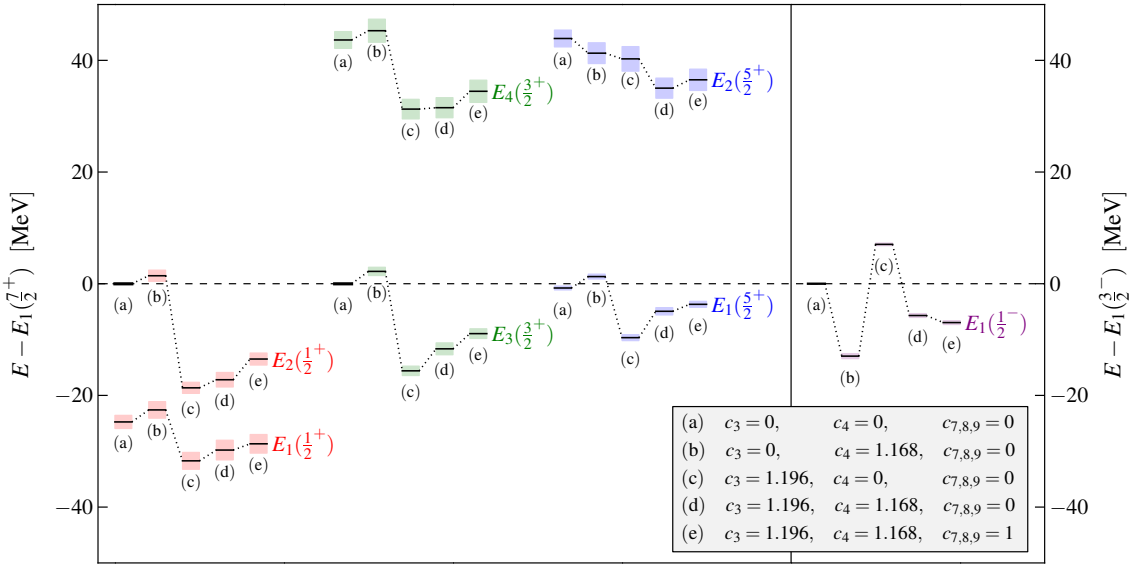

Figure 5: Dependence of the energy splittings $E_n(J^+) - E_1(\frac{7}{2}^+)$ (left) and $E_1(\frac{1}{2}^-) - E_1(\frac{3}{2}^-)$ (right) on the coefficients of the spin-dependent NRQCD interactions [see Eq. (2.2)]. For each energy level, five different choices of coefficients are shown. These results are from the ensemble with $a \approx 0.11$ fm, $am_{u,d} = 0.005$.

As shown in case (c), the operator $\boldsymbol{\sigma}\cdot\left(\widetilde{\boldsymbol{\nabla}}\times\widetilde{\mathbf{E}}-\widetilde{\mathbf{E}}\times\widetilde{\boldsymbol{\nabla}}\right)$ has a large effect on both the positive-parity and negative-parity *bbb* energy splittings, which is of opposite sign to the effect of $\boldsymbol{\sigma}\cdot\widetilde{\mathbf{B}}$. For the multiplet $\{E_2(\frac{1}{2}^+),E_3(\frac{3}{2}^+),E_1(\frac{5}{2}^+),E_1(\frac{7}{2}^+)\}$, which in quark models has $L=2$, $S=\frac{3}{2}$, and a totally symmetric spatial wave function, the energy shifts due to $\boldsymbol{\sigma}\cdot\left(\widetilde{\boldsymbol{\nabla}}\times\widetilde{\mathbf{E}}-\widetilde{\mathbf{E}}\times\widetilde{\boldsymbol{\nabla}}\right)$ are approximately proportional to $2\mathbf{L}\cdot\mathbf{S}=J(J+1)-L(L+1)-S(S+1)$, which is characteristic for a spin-orbit interaction [10].

In case (d), both $\boldsymbol{\sigma}\cdot\widetilde{\mathbf{B}}$ and $\boldsymbol{\sigma}\cdot\left(\widetilde{\boldsymbol{\nabla}}\times\widetilde{\mathbf{E}}-\widetilde{\mathbf{E}}\times\widetilde{\boldsymbol{\nabla}}\right)$ are turned on, and the resulting shifts of the *bbb* energy levels are approximately equal to the sum of the shifts from (b) and (c), but some deviations from linearity can be resolved [4]. Finally, in case (e), the spin-dependent order-v^6 interactions are also included, restoring the full action as used in the main calculations of this work. The *bbb* spin splittings change by up to 30% when these terms are included. A similarly large effect of the order-v^6 terms has also been observed for the bottomonium spin splittings [11].

6. Conclusions

The *bbb* system is an excellent benchmark for nonrelativistic effective field theories and potential models. Here, a precise lattice QCD calculation of *bbb* excited states up to $J=\frac{7}{2}$ was presented. Spin-dependent energy splittings that were neglected in potential models were resolved in this work, and it was shown what contributions these splittings receive from the different NRQCD interactions. The author hopes that these results will stimulate further work on triply heavy baryons using a variety of approaches.

Acknowledgments: This work is supported by the U.S. Department of Energy under cooperative research agreement Contract Number DE-FG02-94ER40818, and was also supported by the U.S. Department of Energy under Grant Number DE-SC0001784.

References

[1] N. Brambilla, A. Vairo, and T. Rosch, Phys. Rev. D **72**, 034021 (2005).

[2] N. Brambilla, J. Ghiglieri, and A. Vairo, Phys. Rev. D **81**, 054031 (2010); F. J. Llanes-Estrada, O. I. Pavlova, and R. Williams, Eur. Phys. J. C **72**, 2019 (2012); N. Brambilla, F. Karbstein, and A. Vairo, arXiv:1301.3013.

[3] S. Meinel, Phys. Rev. D **82**, 114514 (2010).

[4] S. Meinel, Phys. Rev. D **85**, 114510 (2012).

[5] G. P. Lepage *et al.*, Phys. Rev. D **46**, 4052 (1992).

[6] Y. Aoki *et al.* (RBC and UKQCD Collaborations), Phys. Rev. D **83**, 074508 (2011).

[7] R. G. Edwards, J. J. Dudek, D. G. Richards, and S. J. Wallace, Phys. Rev. D **84**, 074508 (2011).

[8] B. Silvestre-Brac, Few-Body Syst. **20**, 1 (1996).

[9] N. Isgur and G. Karl, Phys. Rev. D **18**, 4187 (1978); K.-T. Chao, N. Isgur, and G. Karl, Phys. Rev. D **23**, 155 (1981); D. Gromes, Z. Phys. C **18**, 249 (1983).

[10] D. Gromes and I. O. Stamatescu, Nucl. Phys. B **112**, 213 (1976).

[11] S. Meinel, Phys. Rev. D **82**, 114502 (2010).